EARTHQUAKE ENGINEERING AND STRUCTURAL DYNAMICS
Earthquake Engng Struct. Dyn. 2006; **35**:1699–1719
Published online 6 July 2006 in Wiley InterScience (www.interscience.wiley.com). DOI: 10.1002/eqe.604

Experimental and analytical studies on earthquake resisting behaviour of confined concrete block masonry structures

Norio Hori[1,*,†], Norio Inoue[1], Dangol Purushotam[2], Tetsuya Nishida[3] and Jun Kobayashi[3]

[1]*Department of Architecture and Building Science, Graduate School of Engineering, Tohoku University, Sendai, Japan*
[2]*Department of Earthquake Engineering (Structure), Khwopa Engineering College, Nepal*
[3]*Department of Architecture and Environment Systems, Faculty of Systems Science and Technology, Akita Prefectural University, Yurihonjo, Japan*

SUMMARY

To improve the seismic performance of masonry structures, confined masonry that improves the seismic resistance of masonry structures by the confining effect of surrounding bond beams and tie columns is constructed. This study investigated the earthquake resisting behaviour of confined masonry structures that are being studied and constructed in China. The structural system consists of unreinforced block masonry walls with surrounding reinforced concrete bond beams and tie columns. The characteristics of the structure include: (1) damage to blocks is reduced and brittle failure is avoided by the comparatively lower strength of the joint mortar than that of the blocks, (2) the masonry walls and surrounding reinforced concrete bond beams and tie columns are securely jointed by the shear keys of the tie columns. In this study, wall specimens made of concrete blocks were tested under a cyclic lateral load and simulated by a rigid body spring model that models non-linear behaviour by rigid bodies and boundary springs. The results of studies outline the resisting mechanism, indicating that a rigid body spring model is considered appropriate for analysing this type of structure. Copyright © 2006 John Wiley & Sons, Ltd.

Received 17 June 2005; Revised 6 January 2006; Accepted 28 April 2006

KEY WORDS: confined masonry structure; concrete block; mortar joint; earthquake resistance; static load test; rigid body spring model

*Correspondence to: Norio Hori, Department of Architecture and Building Science, Graduate School of Engineering, Tohoku University, Aoba 6-6-11-1218, Sendai 980-8579, Japan.
†E-mail: hori@struct.archi.tohoku.ac.jp

Contract/grant sponsor: Ministry of Education, Culture, Sports, Science and Technology of Japan
Contract/grant sponsor: Dalian University of Technology, China

1. INTRODUCTION

Masonry structures are used throughout the world for the construction of residential buildings. These days, brick or block masonry structures are most popular in developing countries due to easy handling and inexpensive construction costs. However, structural damage, such as that caused by the 1999 Kocaeli earthquake in Turkey and the 2003 Bam earthquake in Iran, reconfirmed the vulnerabilities of masonry structures without proper reinforcement or confinement, and the urgent necessity for improving the seismic resistance is obvious. To improve the seismic performance of masonry structures, confined masonry that improves seismic resistance by confining effect of the surrounding bond beams and tie columns is prevalent in construction in Latin America and Europe [1].

This study investigated the earthquake resisting behaviour of confined masonry structures that are being studied and constructed in China [2, 3]. This structural system, called 'composite masonry' in China, consists of unreinforced block masonry walls with surrounding reinforced concrete bond beams and tie columns. Figure 1 shows the construction process. (1) The tie column longitudinal reinforcement is anchored to the floor slab. (2) Masonry blocks are placed between the tie columns. Bond beam reinforcement is set on the block walls. (3) Concrete is cast so that the tie columns, bond beams, and walls are securely connected. The characteristics of this structural system are: (1) block damage is reduced and brittle failure is avoided by the comparatively lower strength of the joint mortar than that of the blocks and (2) the masonry walls and surrounding reinforced concrete bond beams and tie columns are securely jointed by the shear keys of the tie columns. This structural system is relatively simple. Any cracking of the walls is delayed and ductility is improved because of the ductile behaviour of the mortar joints and the uniting effect of the post-cast reinforced concrete bond beams and the tie columns with shear keys.

In this study, wall specimens made of concrete blocks were tested under cyclic lateral loads to investigate its earthquake resisting behaviour. The specimens used were half-scale and the variables of the structural parameters used were constant axial load and shear span ratio. An analytical procedure using a rigid body spring model [4, 5] (RBSM) was developed to simulate the experimental results of the specimens. This RBSM can simulate non-linear behaviour such as plasticity, slippage, separation, and recontact by non-linear normal and shear springs distributed over the contact area of two neighbouring rigid bodies.

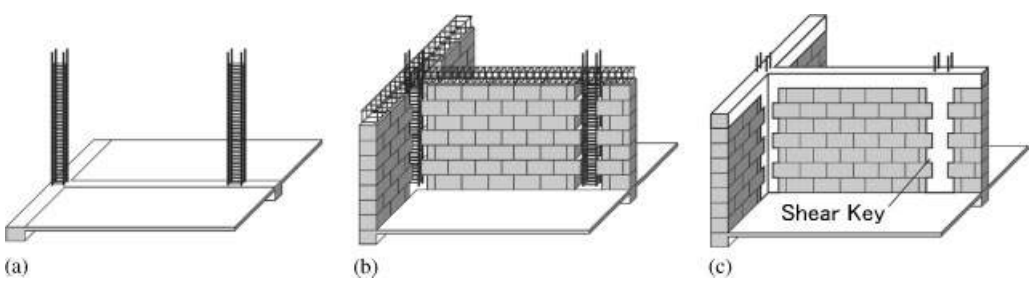

Figure 1. Construction process of the confined masonry in this study: (a) tie column reinforcement; (b) Pile-up blocks and bond beam reinforcement; and (c) casting concrete.

DOI: 10.1002/eqe

2. STATIC LOAD TEST AND RESULTS

2.1. Test specimens and load system

Figure 2 shows the test specimen. The wall was made of concrete blocks without vertical reinforcement and surrounded by a reinforced concrete bond beam and tie columns with shear keys. Shear keys were constructed on the reinforced concrete tie columns for reducing slippage and improving the bond with the concrete blocks. In alternate layers of the concrete block masonry, horizontal connecting bars were provided along the horizontal mortar joints up to 800 mm from the inner sides of both tie columns. One end of each horizontal connecting bar was connected to the tie column reinforcement; the other end was hooked in the joint mortar. The specimen consisted of one bay and one storey, but an additional upper part was attached to the bond beam to distribute the axial load uniformly over the horizontal wall section. The test specimen was constructed at half-scale, but actual sized concrete blocks imported from China were used.

The size of the concrete blocks used was 390 mm × 190 mm × 190 mm and mass is about 18 kg. Each concrete block has two holes (130 mm × 145 mm) on only one side; the other side is flat,

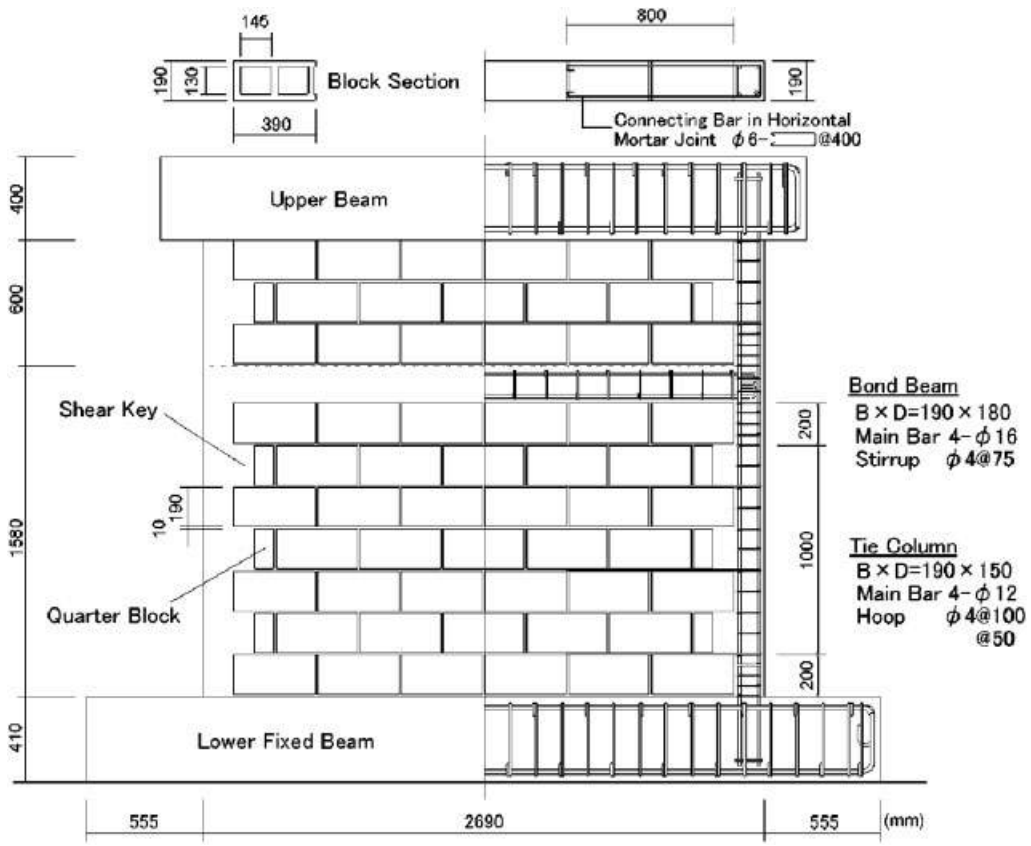

Figure 2. Elevation and reinforcement of the test specimen.

DOI: 10.1002/eqe

Table I. The material properties of the reinforced concrete bond beam and the tie columns.

Main bar of the bond beam	4–ϕ16 (2.35%)
Main bar of the tie columns	4–ϕ12 (1.59%) $\sigma_y = 340\,\mathrm{N/mm^2}$ (by test)
Hoop of the tie columns	ϕ4@100 (0.13%) Centre part ϕ4@50 (0.26%) Top and bottom ends
Strength of the concrete	$\sigma_B = 30.5\,\mathrm{N/mm^2}$ (by test)

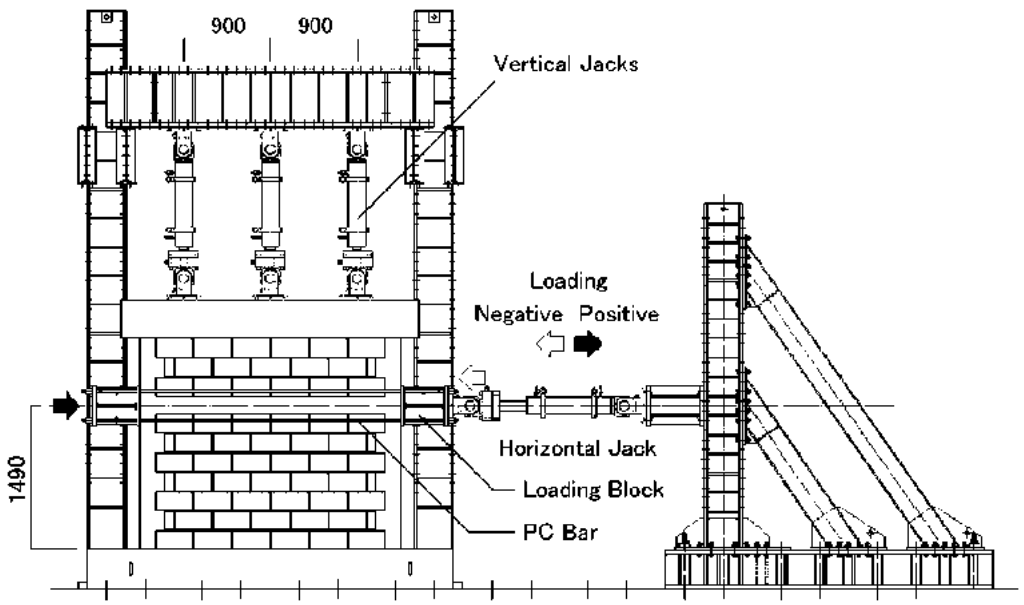

Figure 3. Load system.

with no holes. The holes were ungrouted with mortar or concrete during the construction process. Using the compression test, the strength of the concrete blocks was measured to be $9.4\,\mathrm{N/mm^2}$ for the gross section area, $390\,\mathrm{mm} \times 190\,\mathrm{mm}$.

The material properties of the reinforced concrete bond beam and the tie columns are listed in Table I. The yield stress of the steel and the strength of the concrete were obtained by element tests. The ends of the tie columns had heavier reinforcement to resist shear failure. The spacing between the transverse reinforcement was determined to have an approximate shear reinforcement ratio of 0.2%. The joint mortar, made of cement, lime, and sand in the proportion 1.0:0.65:6.6 was used to construct the concrete block masonry wall.

The load system used for performing the experiment on the specimens is shown in Figure 3. The axial load to simulate a dead load was applied to the specimen by three vertical hydraulic jacks. The static or pseudo-dynamic lateral load [6] to simulate a seismic load was applied by a horizontal hydraulic jack.

DOI: 10.1002/eqe

Table II. Test case.

Test case	Direction of the load	Axial stress σ_N	Shear span ratio M/QD
Case 1	Positive/negative	$0.5\,\mathrm{N/mm^2}$	
Case 2	Negative	0	0.55
	Positive	$1.0\,\mathrm{N/mm^2}$	
Case 3	Positive/negative	$0.5\,\mathrm{N/mm^2}$	1.00

This experiment used three specimens with the same specifications. The test case is shown in Table II. All specimens were tested with a cyclic lateral load, but the constant axial stress and shear span ratio were varied for each test. The jack loads, bond beam horizontal displacements, relative displacements between some concrete blocks, and the strains of the steel reinforcement in the tie columns were measured.

In Case 1, vertical jacks were used to subject the specimen to the constant axial stress of $0.5\,\mathrm{N/mm^2}$, that is the usual value for a first storey in 5-storey masonry structures. The axial stress was equivalently estimated by the gross area of the wall section, which was $2690\,\mathrm{mm} \times 190\,\mathrm{mm}$. In this test case, because the moment was zero at the lateral load height, the shear span ratio $M/QD = H/D = 1490\,\mathrm{mm}/2690\,\mathrm{mm} = 0.55$.

In Case 2, the value of the constant axial stress was changed according to the direction of the lateral load to obtain test data with different structural parameters for the one specimen. That is, during the load in the negative direction, zero axial stress was applied, and during the load in the positive direction, a constant axial stress of $1.0\,\mathrm{N/mm^2}$ was applied to the specimen by three vertical jacks. The direction of the load is shown in Figure 3. In this case, the shear span ratio M/QD was 0.55, the same as in Case 1.

In Case 3, the axial stress was $0.5\,\mathrm{N/mm^2}$, but shear span ratio M/QD was decided to be 1.0 to simulate high-rise structures. In this test case, the moment was assumed to be zero at a height of 2690 mm. The moment equalled QD at the bottom of the masonry wall and $Q(D-H)$ at the lateral load height $H = 1490\,\mathrm{mm}$. To generate this additional moment $Q(D-H)$, the axial loads developed by the vertical jacks were changed as follows:

$$\text{One side jack} \quad N = W/3 \pm Q(D-H)/L$$

$$\text{Centre jack} \quad N = W/3$$

$$\text{Another side jack} \quad N = W/3 \mp Q(D-H)/L$$

N Axial load of each jack

W Total dead load

Q Lateral load by a horizontal jack

D Overall depth of the test specimen (2690 mm)

H Loading height up to a horizontal jack (1490 mm)

L Distance between the side jacks (1800 mm)

The lateral load steps were as follows (see Table III). The horizontal displacement in each load cycle was determined to be small considering that the expected displacement is relatively

DOI: 10.1002/eqe

Table III. Lateral load steps.

Displacement	Drift angle	Cycle
Case 1		
±0.25 mm	±1/6000	2
±0.5 mm	±1/3000	1
±1.5 mm	±1/1000	1
±3 mm	±1/500	2
±6 mm	±1/250	2
±9 mm	±1/167	2
	over +1/100	
Case 2 and Case 3		
∓0.25 mm	∓1/6000	1
∓0.5 mm	∓1/3000	1
∓1.5 mm	∓1/1000	1
∓3 mm	∓1/500	2
∓6 mm	∓1/250	2
∓9 mm	∓1/167	1
−9 mm	−1/167	1
	over +1/100	

small in seismic-resistant design for masonry structures. At first, cyclic loading to achieve a small displacement (horizontal displacement ±0.25 mm or drift angle ±1/6000) was performed to examine elastic stiffness, followed by ±1/3000, ±1/1000, ±1/500, ±1/250, and ±1/167. At the last stage, a positive angle of over 1/100 was performed to investigate the ultimate mechanism. In Cases 2 and 3, the load cycle was started in the negative direction and finished in the positive direction.

2.2. Experimental results

Figure 4 shows the crack pattern after the load test, and lateral load–horizontal displacement relationships measured at the lateral load height.

In Case 1, the initial cracks in the tension side tie column occurred when the drift angle was about 1/5000. With increasing displacement, the resisting force also gradually increased. Stepwise cracks appeared at about 1/1500 and developed towards the compression side of the concrete block masonry wall at about 1/1000. After the load step, the width of the existing vertical cracks and the slippage of the existing horizontal cracks increased, but only few new cracks appeared. Strength was attained at about 1/500 when diagonal cracks went through the concrete blocks on the compression side. The compression side tie column cracked diagonally at about 1/250, and failed at 1/167. However, no drastic decrease in the resisting force occurred up through the last load step.

In the negative load direction of Case 2 (axial stress was zero), the initial cracks in the tension side tie column occurred at about 1/3000. Then, stepwise cracks and horizontal cracks along the bottom section of the masonry wall occurred at about 1/1000. In the positive load direction of Case 2 (axial stress was 1.0 N/mm^2), the initial cracks in the tension side tie column and mortar joints occurred at about 1/1700. Then, development of stepwise cracks, a rapid extension of displacement, and a drastic decrease of resisting force occurred almost simultaneously.

DOI: 10.1002/eqe

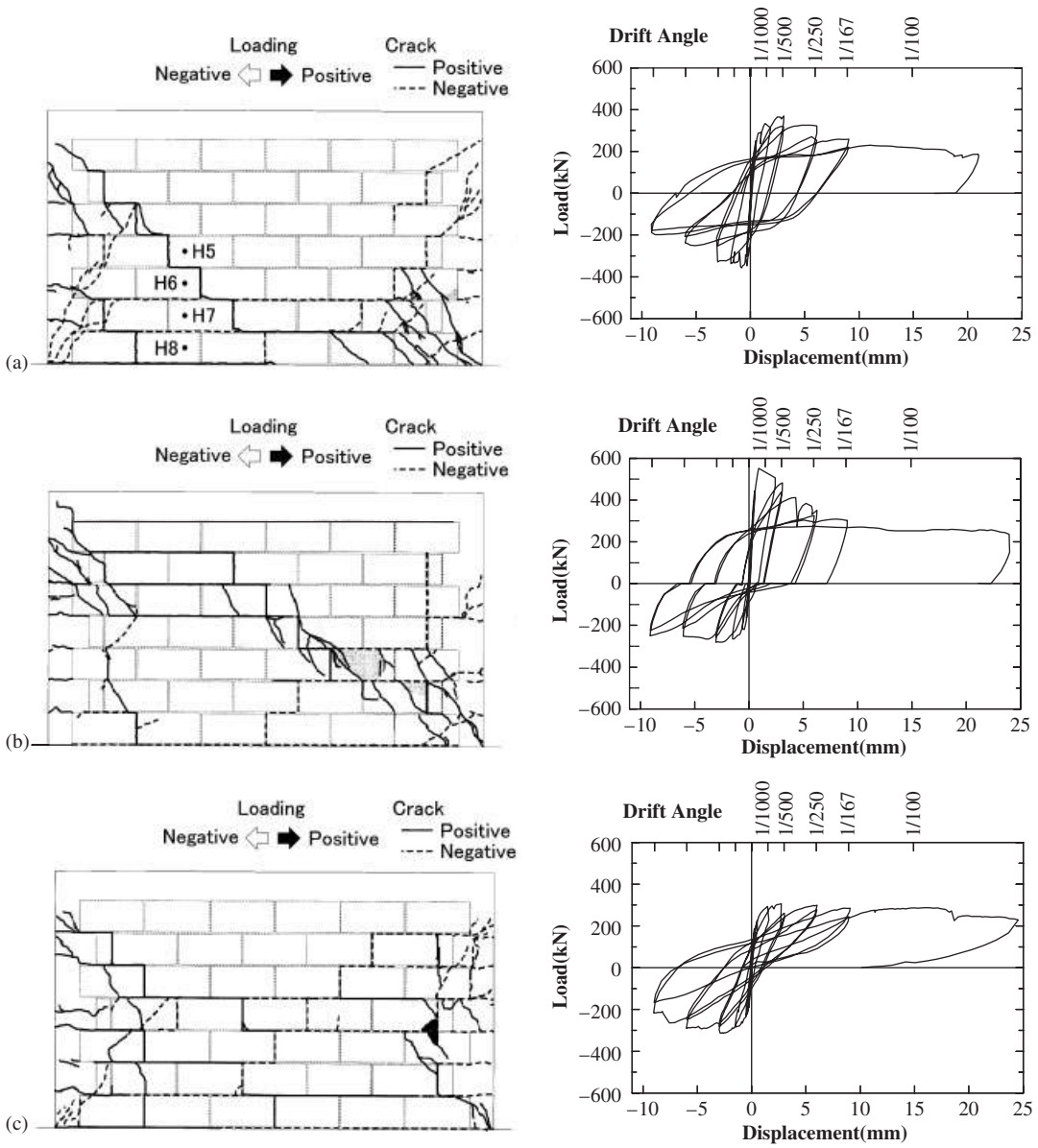

Figure 4. Crack pattern after load test and lateral load–horizontal displacement relationships: (a) Case 1; (b) Case 2; and (c) Case 3.

In the case of loading in the positive direction, the location of the stepwise cracks was higher than that of those in Case 1 and reached the compression side tie column. In the case of loading in the negative direction, the location was lower and reached the bottom centre of the masonry wall.

DOI: 10.1002/eqe

In Case 3, because of the smaller axial stress in the tension side caused by the influence of the shear span ratio, the initial cracks in the tension side tie column occurred at a relatively smaller drift angle of about 1/8000. In the ultimate mechanism, more tension cracks than shear cracks appeared in the tie columns. Although the steel reinforcement in the tension side tie columns did not yield when the strength of the specimen was attained in Cases 1 and 2, yielding was evident in the cycle of 1/500 in Case 3.

As for load–displacement relationship, Case 1 was almost elastic until 1/3000, and then exhibited non-linear behaviour as the number of cracks increased. Although the resisting force decreased gradually under cyclic loading, hysteretic loops of energy dissipation were greater than those in ordinary reinforced concrete walls. It seems that because of the friction stress in the mortar joints after the stepwise cracks occurred, the resisting force was relatively stable even at a large displacement level, and the hysteretic loops were larger.

In Case 2, the maximum resisting force was smaller in loading in the negative direction because of smaller axial stress and larger in loading in the positive direction because of larger axial stress. In both directions, however, the resisting force was relatively stable even at large displacement levels. As for the hysteretic loops, the area was gradually reduced in loading in the negative direction because the stiffness was less due to the smaller axial stress. In Case 3, the hysteretic loops were spindle shaped. Because the cracks in the tie column and the mortar joints on the tension side were relatively large, the resisting force could not increase until after the cracks were closed in the reloading process.

2.3. Lateral load and horizontal displacement of specimens

The load and the displacement of specimens corresponding to the initial crack, stepwise cracks, and maximum load are shown in Tables IV and V, respectively. The load–displacement relationships

Table IV. Load-carrying characteristics of specimens.

Test case	Initial crack load (kN)	Stepwise crack load (kN)	Maximum load (kN)	τ_{max} (N/mm^2)
Case 1	213.6	334.0	370.2	0.72
Case 2, negative	217.2	265.1	281.0	0.55
Case 2, positive	551.1	551.1	551.1	1.08
Case 3	148.1	292.8	314.2	0.61

τ_{max}: Average shear stress of maximum load.

Table V. Horizontal displacement and drift angle of specimens.

Test case	Initial crack	Stepwise crack	Maximum load
Case 1	0.26 mm (1/5731)	1.35 mm (1/1104)	3.09 mm (1/482)
Case 2, negative	0.59 mm (1/2547)	1.46 mm (1/1024)	3.06 mm (1/488)
Case 2, positive	0.89 mm (1/1674)	0.89 mm (1/1674)	0.89 mm (1/1674)
Case 3	0.18 mm (1/8278)	1.47 mm (1/1017)	2.60 mm (1/574)

DOI: 10.1002/eqe

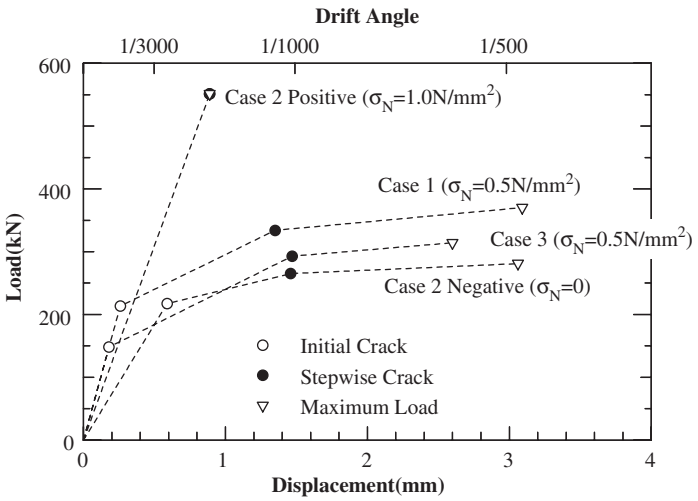

Figure 5. Lateral load and horizontal displacement of specimens.

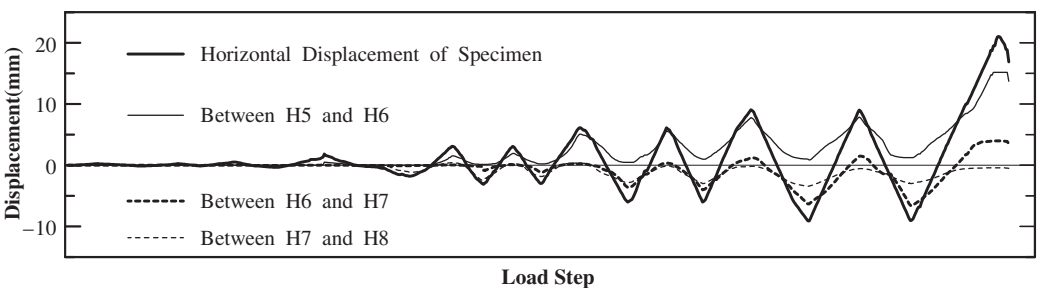

Figure 6. Horizontal displacement of specimen and slippage of mortar joints in test Case 1.

at these three limit states are shown in Figure 5. The maximum load or strength of specimens increased as axial stress increased, and depended primarily on axial stress. Because the resisting force did not increase much after the stepwise cracks occurred, the strength of the specimens is considered to be determined by the strength of the stepwise cracks.

2.4. Slippage of mortar joints

To investigate the slippage of mortar joints, the horizontal displacements between each point, H5, H6, H7, and H8, illustrated in Figure 4(a), are shown in Figure 6, according to the results of Case 1. The abscissa of Figure 6 is the load step, and the horizontal displacement of the specimen is expressed on the ordinates in the same figure. The slippage between H5 and H6, which contains a stepwise crack, had almost the same value as the displacement of the specimen in the case of the positive load step. In the case of the negative load step, the sum of displacements of between

DOI: 10.1002/eqe

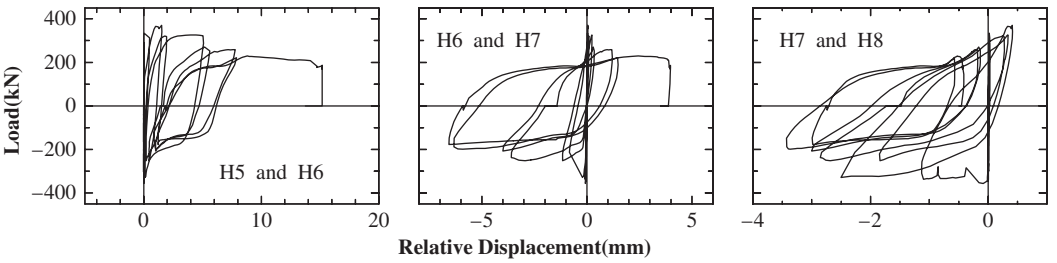

Figure 7. Lateral load of specimen and slippage of mortar joints in test Case 1.

H6 and H7, and between H7 and H8, approximately equalled the displacement of the specimen. This behaviour indicated that the displacement of the specimens was caused primarily by slippage of the mortar joints, not by deformation of the concrete blocks.

The lateral load on the specimen, that related to the shear stress of the mortar joints, and slippage of the mortar joints are shown in Figure 7. The residual slippage of the mortar joints was not cancelled by unloading, and friction occurred along the mortar joints thus leading to a large dissipation of energy. The specimen resisted the load by friction stress of the mortar joints even after cracks appeared, and the friction stress did not decrease because of the normal stress caused by the confinement of the surrounding bond beam and tie columns. Therefore, the resisting force did not decrease to any great degree in the large displacement load step.

3. SIMULATION ANALYSIS

3.1. Rigid body spring model [*4, 5*]

A rigid body spring model (RBSM) consists of a finite number of small rigid bodies connected by normal and shear springs distributed over the contact area of two neighbouring rigid bodies, as shown in Figure 8. Three degrees of freedom, that is, two transitional and one rotational, are defined at the centre point of each rigid body. In general, and in this study, the centre of mass is used as the centre point. The movement of the rigid body defines the response of the springs distributed over the boundaries of the two neighboring rigid bodies. The response of the spring model provides the interaction between the rigid bodies instead of the internal behaviour of each rigid body. Therefore, this model is appropriate for problems where material discontinuities are dominant such as the non-linear behaviour of metallic materials and the breaking behaviour of rocks.

Figure 9 shows the relative displacement of the boundary element between two rigid bodies. In the model formulation, the rigid bodies are separated both horizontally and vertically, and then, each rigid body rotates at its centre point. Using these displacements, the relative displacements of the two rigid bodies, that is, the displacements of the normal and shear springs, are defined. The relative displacement of the normal and shear springs, $\delta_n(x, y)$ and $\delta_s(x, y)$ on a point $\mathrm{P}(x, y)$ are defined by the product of the geometrical matrix $[B(x, y)]$ and the displacements of the centre

DOI: 10.1002/eqe

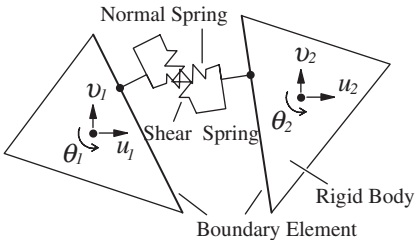

Figure 8. Rigid body spring model.

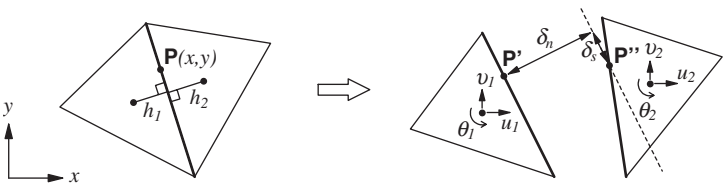

Figure 9. Displacements of rigid bodies and a boundary element.

points of rigid bodies $\{u\}$, as follows:

$$\begin{Bmatrix} \delta_n(x, y) \\ \delta_s(x, y) \end{Bmatrix} = [B(x, y)]\{u\} = [B(x, y)] \begin{Bmatrix} u_1 \\ v_1 \\ \theta_1 \\ u_2 \\ v_2 \\ \theta_2 \end{Bmatrix} \tag{1}$$

The increment of the stress in the normal and shear spring, $\Delta\sigma_n(x, y)$ and $\Delta\tau_s(x, y)$, are defined by Equation (2).

$$\begin{Bmatrix} \Delta\sigma_n(x, y) \\ \Delta\tau_s(x, y) \end{Bmatrix} = [D] \begin{Bmatrix} \Delta\delta_n(x, y) \\ \Delta\delta_s(x, y) \end{Bmatrix} \tag{2}$$

where $[D]$ is the constitutive matrix and, in the case of an elastic condition, is given by Equation (3).

$$[D] = \begin{bmatrix} k_n & 0 \\ 0 & k_s \end{bmatrix} \tag{3}$$

where k_n and k_s are the elastic stiffness normalized by area, of normal and shear springs, respectively. The dimensions of the stiffness, therefore, [stiffness]/[area] = [force]/[length]^3.

DOI: 10.1002/eqe

To formulate k_n and k_s, the equivalent normal and shear strains, ε_n and γ_s are assumed by the perpendicular distance between boundary and the centre point of each rigid body, as follows, h_1 and h_2 in Figure 9.

$$\begin{Bmatrix} \varepsilon_n \\ \gamma_s \end{Bmatrix} = \frac{1}{h_1 + h_2} \begin{Bmatrix} \delta_n \\ \delta_s \end{Bmatrix} \tag{4}$$

By considering the plane stress condition, the normal and shear stress–strain relationship is given as follows by the tangential modulus of elasticity E and Poisson's ratio v.

$$\begin{aligned} \sigma_n &= \frac{E}{1 - v^2} \varepsilon_n \\ \tau_s &= \frac{E}{1 + v} \gamma_s \end{aligned} \tag{5}$$

Thus, the elastic stiffness of normal and shear springs, k_n and k_s are defined as follows:

$$\begin{aligned} k_n &= \frac{\sigma_n}{\delta_n} = \frac{E}{1 - v^2} \frac{1}{h_1 + h_2} \\ k_s &= \frac{\tau_s}{\delta_s} = \frac{E}{1 + v} \frac{1}{h_1 + h_2} \end{aligned} \tag{6}$$

The shear springs provided in the boundary element of the two rigid bodies represents the shear transferring mechanism of the joint mortar. The shear slip surface is based on the normal and shear stress of each boundary element. Shear slip occurs after reaching the shear yielding strength given by Mohr–Coulomb's equation and develops along the shear slip surface with a changing constitutive matrix according to the flow rule of plasticity. Using the flow rule on the slip surface caused by shearing, the following yield function f is assumed to define the constitutive equation for the post-yielding stage.

$$f = {\tau_s}^2 - (c - \sigma_n \tan \phi)^2 \tag{7}$$

where c is cohesion and ϕ is the angle of internal friction. The following equation is given in the orthogonal condition:

$$\frac{\partial f}{\partial \sigma_n} \Delta \sigma_n + \frac{\partial f}{\partial \tau_s} \Delta \tau_s = 0 \tag{8}$$

By solving the above equations, the constitutive matrix after yielding is defined by the following equations:

$$[D] = \begin{bmatrix} k_n & 0 \\ 0 & k_s \end{bmatrix} - [S] \tag{9}$$

$$[S] = \frac{1}{F} \begin{bmatrix} \{(c - \sigma_n \tan \phi) \tan \phi\}^2 {k_n}^2 & (c - \sigma_n \tan \phi) \tan \phi \, k_n \tau_s k_s \\ (c - \sigma_n \tan \phi) \tan \phi \, k_n \tau_s k_s & {\tau_s}^2 {k_s}^2 \end{bmatrix} \tag{10}$$

$$F = \{(c - \sigma_n \tan \phi) \tan \phi\}^2 k_n + {\tau_s}^2 k_s \tag{11}$$

DOI: 10.1002/eqe

By the external force $\{P\} = \{X_1, Y_1, M_1, X_2, Y_2, M_2\}^{\mathrm{T}}$ and the displacement $\{u\}$ at the centre point of the rigid bodies, the external work of the rigid bodies and the internal work of the boundary element become as follows according to the virtual work theory:

$$\{u^*\}^{\mathrm{T}}\{P\} = \int_A \begin{Bmatrix} \delta_n^* \\ \delta_s^* \end{Bmatrix}^{\mathrm{T}} \begin{Bmatrix} \sigma_n \\ \tau_s \end{Bmatrix} \mathrm{d}A \tag{12}$$

where $\{u^*\}$ is virtual displacement of rigid bodies, δ_n^* and δ_s^* are virtual displacement of normal and shear springs, and A is the variable area of the boundary element. By replacing $\{\sigma_n, \tau_s\}$ with $\{\delta_n, \delta_s\}$ by Equation (2) and $\{\delta_n, \delta_s\}$ with $\{u\}$ by Equation (1), the following equations are given.

$$\{P\} = [K]\{u\} \tag{13}$$

$$[K] = t \int_s [B(x, y)]^{\mathrm{T}}[D][B(x, y)]\,\mathrm{d}s \tag{14}$$

where t is the thickness of the boundary element and rigid bodies, and s is the variable length of the boundary element.

As for steel reinforcement, element stiffness matrix $[K_s]$ of the boundary element is constructed separately from that for concrete. Afterward, it is added to that of the concrete. The steel reinforcement is assumed to follow a smeared model that has one-directional stiffness, and the stress–strain relationship is assumed to be an elasto-plastic bilinear model. Constitutive matrix $[D_s]$ of the steel reinforcement is given by following equations.

$$\begin{aligned} &\text{Elastic condition} \quad [D_s] = \frac{E_s \cos^2\theta}{h_1 + h_2} \begin{bmatrix} \cos^2\theta & -\cos\theta\sin\theta \\ -\cos\theta\sin\theta & \sin^2\theta \end{bmatrix} \\ &\text{Post-yielding} \qquad [D_s] = \begin{bmatrix} 0 & 0 \\ 0 & 0 \end{bmatrix} \end{aligned} \tag{15}$$

where E_s is the modulus of elasticity of the steel reinforcement and θ is the angle between the direction of reinforcement and the normal direction of the boundary element.

3.2. Analysis model of test specimen

The test specimen was divided into rectangular and triangular rigid bodies, as shown in Figure 10. Because cracking of the mortar joints was found to be dominant in the experiments, one concrete block was modelled as a rectangular rigid body and a typical rigid body was surrounded by six boundary elements, as shown in Figure 10. Reinforced concrete bond beam and tie columns were modelled as rectangular rigid bodies except for the top and bottom ends of the tie columns, which were modelled by triangular rigid bodies to enable simulation of the inclined shear cracks and the failure. The steel reinforcements in the bond beam and tie columns were included in the analysis model. Horizontal connecting bars in the horizontal mortar joints would be useful for maintaining the integrity of a masonry wall after diagonal cracking, but there was little contribution to stiffness

DOI: 10.1002/eqe

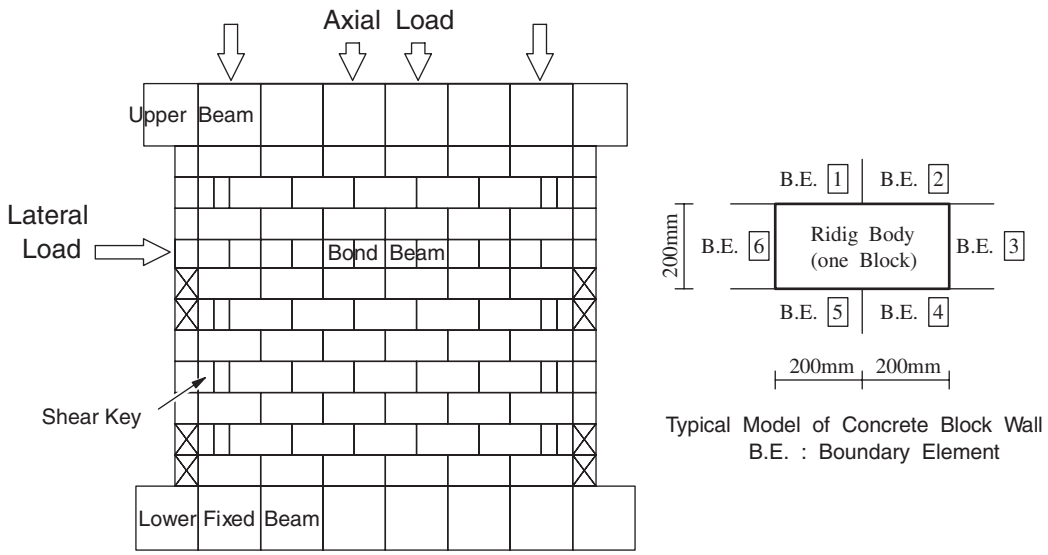

Figure 10. Analysis model of test specimen.

and strength because plain round bar, which had a low bond stress, was used. Therefore, horizontal connecting bars were neglected in this analysis model.

Although an axial load was applied by using three vertical jacks in the load tests, four load points were used in the analysis model for the convenience of modelling. A lateral load was applied to the side of a tie column at the bond beam, and the resisting behaviour was investigated by one-direction pushover analysis.

3.3. Constitutive model of materials

A constitutive model of joint mortar was determined from the three concrete block element load tests, as illustrated in Figure 11. The compression test shown in Figure 11(a) was used to measure normal stiffness and normal strength. The shear test shown in Figure 11(b) was used to measure the shear strength of the joint mortar under constant normal stress, 0.25, 0.5, 1.0 and 1.5 N/mm^2.

Figure 12 shows axial load–vertical displacement relationship of the compression test. Vertical displacement was measured between the two points shown in Figure 11(a). The concrete blocks suffered almost no damage up to the maximum load of the test. Accordingly, the strength of these specimens depended on the strength of the joint mortar. From this result, the normal compressive strength $\sigma_B = 4.8\,N/mm^2$ and Young's modulus $E = 5.4 \times 10^3\,N/mm^2$ were measured for the joint mortar. These two values were evaluated using the gross section area of the concrete block, 390 mm × 190 mm. The strength of the concrete blocks was 9.4 N/mm^2, as mentioned in Section 2.1, and therefore, the strength of the joint mortar was about half that of the concrete blocks. Normal stress–strain relationship of joint mortar is assumed and indicated by the solid line in Figure 13. Tension strength was assumed as $0.1\sigma_B$.

The normal stress–strain relationship of the concrete used in the surrounding bond beam and tie columns was assumed and indicated by the broken line in Figure 13. Under compressive

DOI: 10.1002/eqe

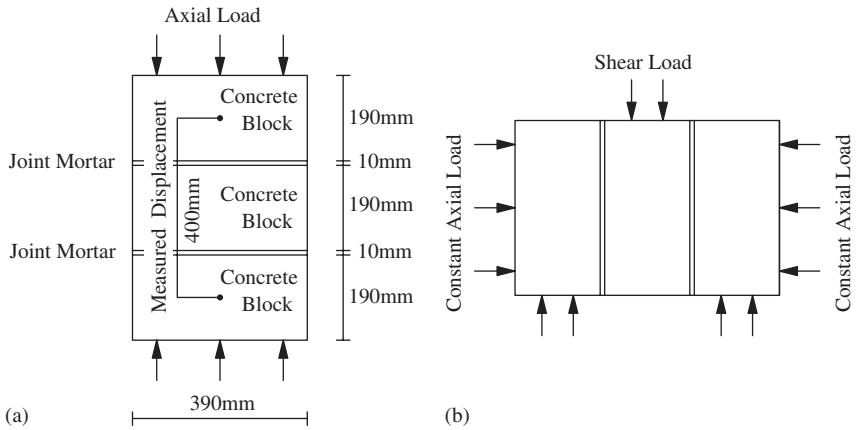

Figure 11. Illustration of the three concrete block element load tests: (a) compression test; and (b) shear test.

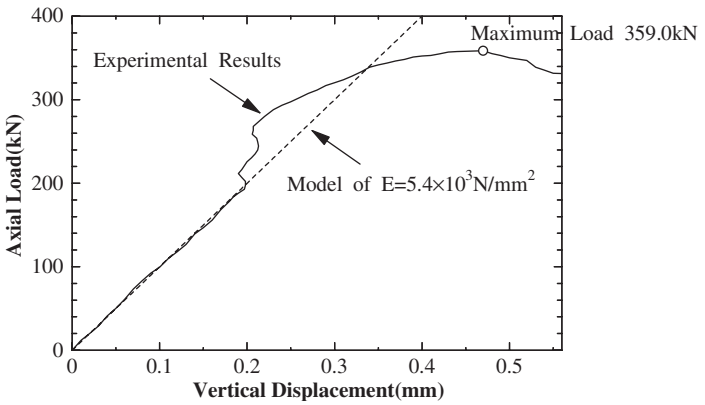

Figure 12. Axial load–vertical displacement relationship of compression test.

conditions, first yielding occurs and tangential modulus becomes $0.5E$ when the stress becomes $0.5\sigma_B$. Under tensile conditions, the tension strength was assumed as $0.1\sigma_B$. Then, the tension stiffening effect was applied in the case that the steel reinforcement crossed the concrete boundary element perpendicularly.

Through the shear test, the shear strength obtained under constant normal stress is plotted by the marks in Figure 14. Based on these results, Mohr–Coulomb's shear yield surface was assumed by cohesion $c = 0.235\,\mathrm{N/mm^2}$ and internal friction angle $\phi = 24.0°$. In the simulation analysis, shear slip occurs and the $[D]$ matrix is reconstructed by Equation (9) when shear stress reaches this shear slip surface.

The stress–strain relationship of the steel reinforcement was assumed as an elasto-plastic bilinear model with Young's modulus $E_s = 210 \times 10^3\,\mathrm{N/mm^2}$ and yield stress $\sigma_y = 340\,\mathrm{N/mm^2}$.

DOI: 10.1002/eqe

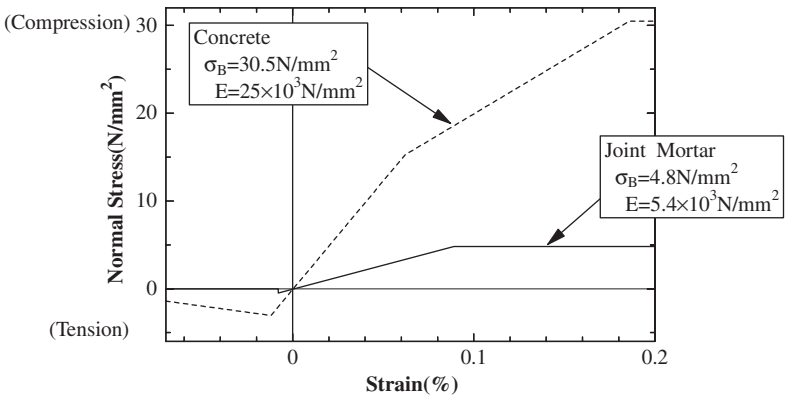

Figure 13. Stress–strain model of normal springs.

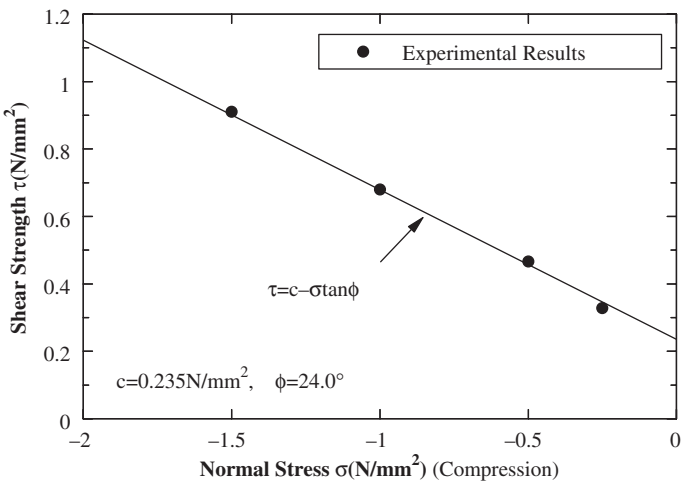

Figure 14. Normal stress–shear strength relationship of the joint mortar.

3.4. Consideration of analytical results

The RBSM simulation results are discussed below. The non-linear responses of the specimens were computed through a process of incremental analysis. The Newton–Raphson iteration method was used to release the unbalanced forces caused by non-linearity. Figure 15 shows lateral load–horizontal displacement relationship and deformation at maximum load, corresponding with the test cases. In the load–displacement relationship, the fine lines are the test results until the load step of 1/500 drift angle, and the bold lines are the results of RBSM analysis before numerical overflow by the collapse mechanism. In the deformation figure, the deformation scale is 100 times larger than the specimen scale.

Figure 15(a) shows the results corresponding to test Case 1. RBSM almost exactly simulated the initial stiffness and the strength. The deformation figure shows the rotation and tension cracks of

DOI: 10.1002/eqe

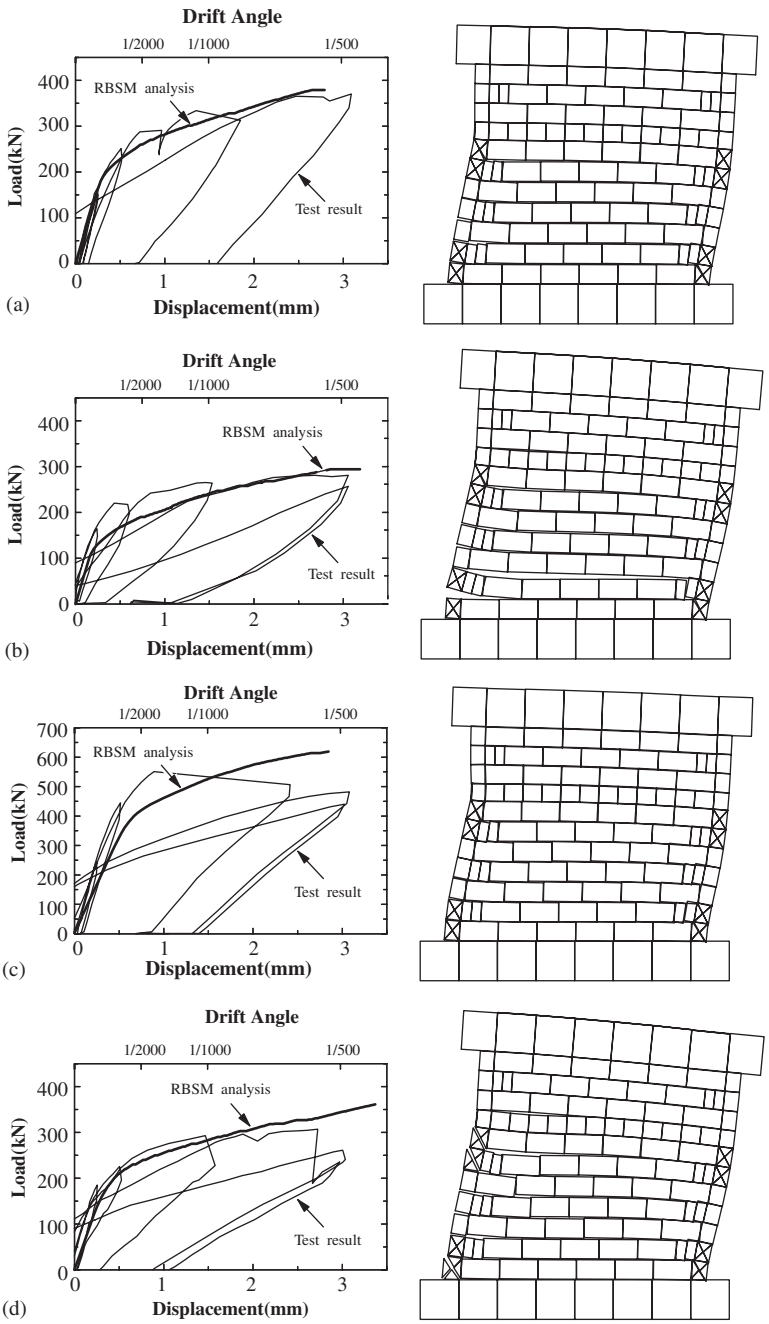

Figure 15. Lateral load–horizontal displacement relationshipand deformation at maximum load: (a) $\sigma_N = 0.5\,\mathrm{N/mm^2}$, $M/QD = 0.55$ (Case 1); (b) $\sigma_N = 0$, $M/QD = 0.55$ (Case 2, negative direction); (c) $\sigma_N = 1.0\,\mathrm{N/mm^2}$, $M/QD = 0.55$ (Case 2, positive direction); and (d) $\sigma_N = 0.5\,\mathrm{N/mm^2}$, $M/QD = 1.0$ (Case 3).

DOI: 10.1002/eqe

the tension side tie column, the rotation and shear failure of the compression side tie column, and slippage of the mortar joints. Regarding the results of analysis, slippage cracks began to appear at the applied load equal to about 140 kN (drift angle 0.14/1000) and developed towards the almost horizontal mortar joints at the applied load of about 200 kN (drift angle 0.23/1000) with a decrease in the stiffness of specimen. After that, the masonry wall was mostly deformed by the shear slippage of the horizontal mortar joints. The initial tension cracks of the tension side tie column occurred when the load of 250 kN (drift angle 0.44/1000) was reached. Shear yielding of the mortar joints then appeared and stepwise cracks were dominant at about 360 kN (drift angle 1.5/1000). The inclined boundary elements of the compression side tie column slipped at the maximum load of 379 kN (drift angle 1.8/1000), and the specimen failed to the collapse mechanism.

Figures 15(b) and (c) show the results corresponding to test Case 2. In cases with vertical axial loads, (a) and (c), the collapse mechanism was shear slippage of the mortar joints and inclined shear failure of the compression side tie column. However, in the case with no vertical axial load, (b), the entire masonry wall rotated and mortar joint tension cracks occurred on the lower layer of the wall. Strength increased with a larger vertical axial load in the experimental load test because of the higher shear resistance of the mortar joints; this strengthening effect was simulated by RBSM analysis.

Figure 15(d) shows the results corresponding to test Case 3. Because of the smaller axial stress at the tension side of wall by the additional moment load, shear slippage appeared easily. The strength was less than in case (a). Almost all the mortar joints slipped by shear yielding near the maximum load in cases (a) and (c), but tension cracks also appeared on the tension side of the wall in case (d).

Figure 16 shows the resultant stress of normal and shear stress distributed on each boundary element at the maximum load. Against the lateral load, the structural system was considered to resist by inclined compressive force consisting of normal and shear stress between the concrete blocks and mortar joints. Larger normal stress σ_N increased the inclined compressive force of concrete block masonry wall because the shear stress of the mortar joints increased. On the tension side of the wall, only tie column reinforcement resisted the tension force by the overturning moment. It is considered that the stability of the hysteretic loop is given by the shear resistance of mortar joints and that the force between a masonry wall and the surrounding reinforced concrete bond beam and tie columns is effectively transferred because of the uniting effect of post-casting and shear keys.

3.5. Relationship between strength and structural conditions

The relationship between strength and structural conditions were investigated by RBSM analysis. The parameter variables were axial stress and shear span ratio. In Figure 17, the ordinates are shear strength, i.e. the maximum lateral load divided by the gross section area of the wall, 2690 mm × 190 mm. The case of the figure on the left has the same shear span ratio and different axial stresses. The case of the figure on the right has the same axial stress and different shear span ratios. RBSM analysis gave good results compared with the test ones, which are plotted by triangle marks in Figure 17.

In the case of different axial stresses, as shown in the figure on the left, the shear strength increased with larger axial stress because the shear strength of the mortar joints increased.

In the case of different shear span ratios, as shown in the figure on the right, the shear strength decreased with larger shear span ratio, where the shear span ratio of 0.55 corresponds to a 2- or 3-storey, 1.0 corresponds to a 5- or 6-storey, and 1.5 corresponds to a 7- or 8-storey building in

DOI: 10.1002/eqe

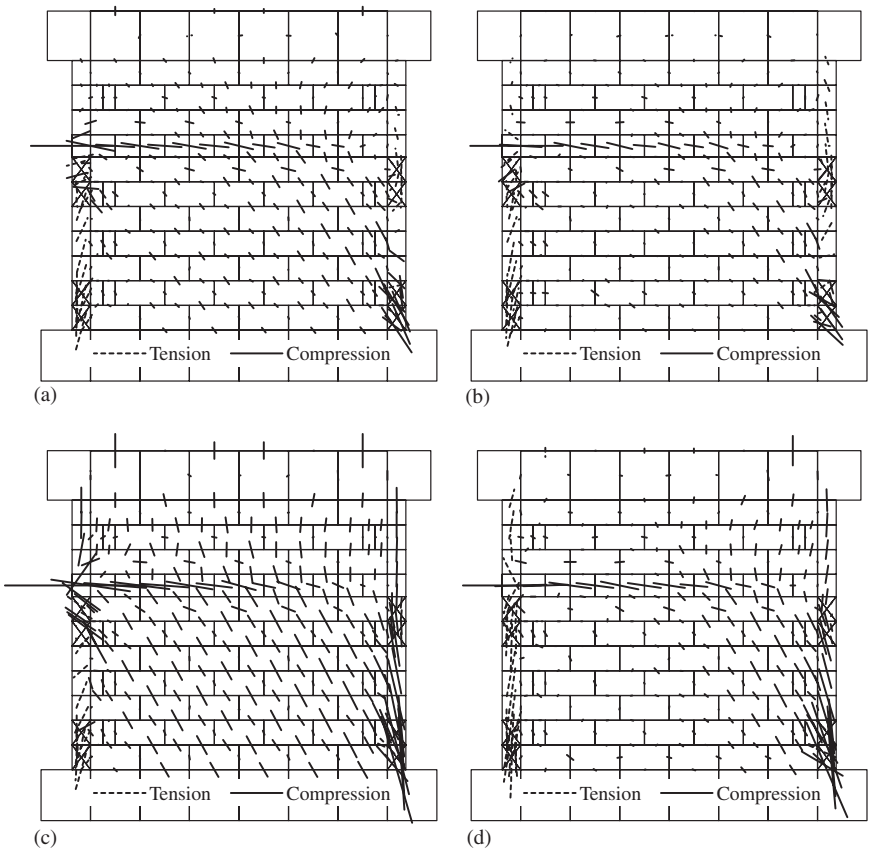

Figure 16. Stress distribution at maximum load: (a) $\sigma_N = 0.5\,\mathrm{N/mm^2}$, $M/QD = 0.55$ (Case 1); (b) $\sigma_N = 0$, $M/QD = 0.55$ (Case 2, negative direction); (c) $\sigma_N = 1.0\,\mathrm{N/mm^2}$, $M/QD = 0.55$ (Case 2, positive direction); and (d) $\sigma_N = 0.5\,\mathrm{N/mm^2}$, $M/QD = 1.0$ (Case 3).

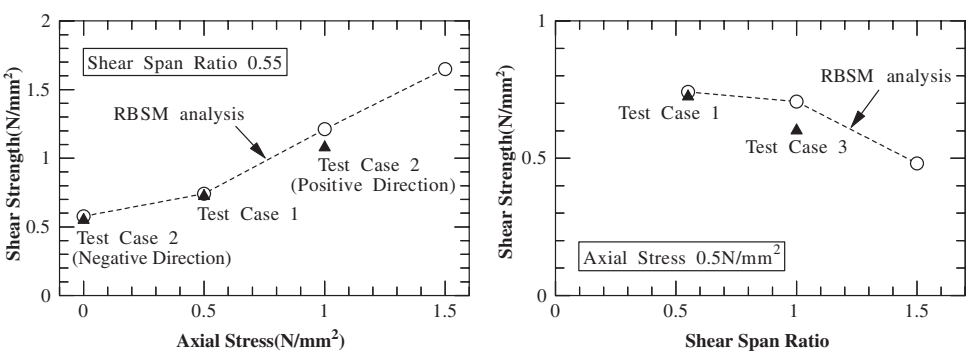

Figure 17. Strength and structural conditions.

DOI: 10.1002/eqe

general. In case of high-rise buildings, the shear strength of the mortar joints decreases because of the tension stress by the overturning moment. Therefore, the strength and the energy-dissipating capacity of buildings are considered to become smaller.

4. CONCLUSIONS

In this study, load tests and simulation analyses were use to investigate the earthquake resisting behaviour of confined masonry walls made of concrete blocks. This structural system is simple but has relatively better seismic performance.

By experimental studies, it was found that the horizontal deformation of specimens primarily occurred by the slippage of mortar joints, and that the resisting force was relatively stable even with large displacement levels and the hysteretic loops were relatively large. The unloading process did not cancel the residual slippage of mortar joints. The specimen then resisted the lateral load by friction stress of the mortar joints even after cracks occurred. Therefore, the resisting force did not decrease drastically even in a large displacement load step, and ductile behaviour could be expected. Damage of the concrete blocks was reduced and brittle failure was avoided by comparatively lower strength and ductile behaviour of the joint mortar. By the uniting effect of post-cast reinforced concrete bond beam and tie columns with shear keys, the force between the masonry wall and the surrounding reinforced concrete bond beam and tie columns was effectively transferred in this structural system. The collapse mechanism of this structural system was the shear slippage of the mortar joints, the shear failure of the compression side tie column, and the tension yielding of the steel reinforcement in the tension side tie column.

In this study, the rigid body spring model (RBSM) was used for the simulation analysis, and good results were obtained compared with the test results. This RBSM consists of a finite number of small rigid bodies and boundary elements between every neighbouring rigid body. Accordingly, this model is suitable for simulating the non-linear behaviour of mortar joints. Applying Mohr–Coulomb's yield surface to the inelastic rule of joint mortar enabled appropriate evaluation of the influence of axial load on shear strength.

The resisting mechanism of this structural system on the lateral load is a combination of tension force in the tension side tie column and inclined compressive force in a concrete block masonry wall that is the resulting force of normal and shear stress on mortar joints. Therefore, the strength of this structural system is primarily controlled by the inclined compressive force on a masonry wall and the tension strength of tie column reinforcement. In the case of a small dead load or large axial stress on the tension side as a consequence of the overturning moment in high-rise buildings, earthquake-resistant design must consider a lower shear resisting capacity of a block masonry wall, such as the strength and energy-dissipating capacity.

ACKNOWLEDGEMENTS

This study was a part of the research project [7], 'Development of Earthquake and Tsunami Disaster Mitigation Technologies and Its Integration for the Asia-Pacific Region (Chairman, Prof. Kameda, Hiroyuki)' sponsored by the Ministry of Education, Culture, Sports, Science and Technology of Japan. This study was also completed in co-operation with Dalian University of Technology, China.

DOI: 10.1002/eqe

REFERENCES

1. Tomaževič M. Recent advances in earthquake-resistant design of masonry buildings: European prospective. *Eleventh World Conference on Earthquake Engineering*, *Paper No. 2012*, 1996.
2. Wu RF. The state-of-arts of the masonry structures in China. *Proceedings of the 11th International Brick/Block Masonry Conference*, Supplementary Volume, 1997; 1–6.
3. Wu RF, Zhang QG. Medium and high-rise masonry construction in China—research and application of composite masonry wall system. *Proceedings of the 11th World Conference on Earthquake Engineering*, *Paper No. 662*, 1996.
4. Kawai T. New element models in discrete structure analysis. *Journal of Society of Naval Architects of Japan* 1977; **141**:174–180.
5. Kei T, Ueda M, Kawai T. Nonlinear analysis of a reinforced concrete shear wall by rigid body spring models. *Transactions of the JCI* 1985; **7**:449–456.
6. Nishida T, Teramoto N, Kobayashi J, Inoue N, Hori N, Cai X. Seismic response estimation of composite masonry structure by equivalent linearization method. *13th World Conference on Earthquake Engineering*, *Paper No. 3067*, 2004.
7. EqTAP project web site, http://eqtap.edm.bosai.go.jp/index.html, Earthquake Disaster Mitigation Research Center—NIED.

DOI: 10.1002/eqe